Journal of Neurochemistry JNC

JOURNAL OF NEUROCHEMISTRY | 2017 | 140 | 613–628 doi: 10.1111/jnc.13921

ORIGINAL ARTICLE

Network-based characterization of the synaptic proteome reveals that removal of epigenetic regulator *Prmt8* restricts proteins associated with synaptic maturation

Patrick Kia Ming Lee,*,†,‡ Wilson Wen Bin Goh‡,§ and Judy Chia Ghee Sng†

*Integrative Neuroscience Program, Singapore Institute for Clinical Sciences, Agency for Science Technology and Research (A*STAR), Singapore

†Department of Pharmacology, Yong Loo Lin School of Medicine, National University of Singapore, Singapore

‡School of Pharmaceutical Science and Technology, Tianjin University, Tianjin, China

§Department of Computer Science, National University of Singapore, Singapore

Abstract

The brain adapts to dynamic environmental conditions by altering its epigenetic state, thereby influencing neuronal transcriptional programs. An example of an epigenetic modification is protein methylation, catalyzed by protein arginine methyltransferases (PRMT). One member, *Prmt8,* is selectively expressed in the central nervous system during a crucial phase of early development, but little else is known regarding its function. We hypothesize *Prmt8* plays a role in synaptic maturation during development. To evaluate this, we used a proteome-wide approach to characterize the synaptic proteome of *Prmt8* knockout versus wild-type mice. Through comparative network-based analyses, proteins and functional clusters related to neurite development were identified to be differentially regulated between the two genotypes. One interesting protein that was differentially regulated was tenascin-R (TNR). Chromatin immunoprecipitation demonstrated binding of PRMT8 to the *tenascin-r* (*Tnr*) promoter. TNR, a component of perineuronal nets, preserves structural integrity of synaptic connections within neuronal networks during the development of visual-somatosensory cortices. On closer inspection, *Prmt8* removal increased net formation and decreased inhibitory parvalbumin-positive (PV+) puncta on pyramidal neurons, thereby hindering the maturation of circuits. Consequently, visual acuity of the knockout mice was reduced. Our results demonstrated *Prmt8*'s involvement in synaptic maturation and its prospect as an epigenetic modulator of developmental neuroplasticity by regulating structural elements such as the perineuronal nets.

Keywords: neuroepigenetics, perineuronal nets, protein arginine methyltransferase, proteomics, tenascin-r, visual cortex.

J. Neurochem. (2017) **140**, 613–628.

Neuroepigenetics is the study of modifications to chromatin in neural cells that does not affect the genotype. In a system consisting of predominantly non-dividing cells, epigenetics provide a logical response mechanism by altering and regulating transcriptional efficiency of the neural cell to the changing environment and its stimuli. Many studies have shown that neuronal activity arising from environmental challenge induces changes to DNA and histone patterns in important neurological processes (Korzus *et al.* 2004; Levenson *et al.* 2004; Miller and Sweatt 2007; Putignano *et al.* 2007; Dash *et al.* 2009;

Received October 8, 2016; revised manuscript received November 30, 2016; accepted December 4, 2016.

Address correspondence and reprint requests to Wilson Wen Bin Goh, School of Pharmaceutical Science and Technology, Tianjin University, 92 Weijin Road, Nankai District, Tianjin 300072, China. E-mail: wilson.goh@tju.edu.cn; goh.informatics@gmail.com

(or)

Judy Chia Ghee Sng, Department of Pharmacology, Yong Loo Lin School of Medicine, National University of Singapore, MD3, 16 Medical Drive #04-01 Singapore 117600. E-mail: phcsngj@nus.edu.sg

Abbreviations used: iTRAQ, isobaric tags for absolute and relative quantification; PRMT, protein arginine methyltransferase; PV/PV+, parvalbumin/parvalbumin-positive; TNR, tenascin-R; VWT, visual water task.

Guan *et al.* 2009; Ma *et al.* 2009; Gupta *et al.* 2010; Brunner *et al.* 2012).

During early stages of neurodevelopment, the juvenile neocortex displays enhanced neuroplasticity and synaptic pruning, driven by molecular changes at the synaptic level (Dahlhaus *et al.* 2011). Synaptic plasticity or changes in efficiency of communication between neurons reflects adaptive brain function and often associated with learning. Long-term functional consequences of neuronal activity are changes in protein synthesis (Sutton *et al.* 2004, 2006). Long-lasting changes to synaptic connections (synaptic remodeling) are often accompanied by changes in the proteins involved in receptor (Ju *et al.* 2004), ion channel densities (Raab-Graham *et al.* 2006) or dendritic spine dynamics (Engert and Bonhoeffer 1999). Such alterations are not only limited to protein turnover but also to post-translational modifications and subcellular relocalization (Rosenberg *et al.* 2014; Alberini and Kandel 2015). These, in turn, underlie many neuronal diseases (Rosenberg *et al.* 2014) and are associated with synaptopathies, such as autism or schizophrenia (Grant 2012). Therefore, synaptic proteome characterization is critical.

Since packaged/processed proteins are exported into the synaptic space, proteomics, the high-throughput study of proteins, provides direct evidence on the protein profiles (identities and expression levels). Unfortunately, studying the synaptic proteome is difficult because of biological and platform-specific problems. In the former, insufficient protein concentrations and high amounts of irrelevant proteins, contribute toward biological noise, and confounds analysis (Karp *et al.* 2010). In the latter, contemporary proteomics is affected by issues such as incomplete coverage and intersample inconsistency (during protein identification), and quantitation instability (Goh *et al.* 2012; Goh and Wong 2014). In data-dependent acquisition-based proteomics, different peptide precursors identified in the first round of mass spectrometry (MS) are semi-randomly selected for fragmentation and analysis in MS/MS space, leading to the identification of different peptides, and therefore, proteins (Goh *et al.* 2013b). Even for the same sample, re-running it multiple times will lead to acquisition of spectra originating from different peptides/proteins. Mapping raw spectra against theoretical protein sequence libraries is also problematic: in practice, only a small part of acquired spectra are confidently assigned to peptides (Lluch-Senar *et al.* 2016). Moreover, running different library-search algorithms may result in different proteins being identified, especially among low confidence proteins (low unique peptide support) (Nesvizhskii 2007). Since peptides are identified semi-randomly, and cannot be consistently assigned to real sequences, protein expression is consequently determined by different constituent peptides per sample. Although this may be ameliorated via unbiased tagging procedures, e.g. isobaric tags for absolute and relative quantification (iTRAQ) or tandem mass tags (TMT), low abundance and proteins with low peptide support should be dealt with cautiously.

There are many efforts to improve synaptic proteome characterization. Liu *et al.* (2014) used antibody-based immunoprecipitation techniques to bind and concentrate proteins or protein complexes associated with Kif5C followed by gel fractionation and then LC-MS analysis. However, while techniques that rely on immunoprecipitation help improve data purity, and thus analytical outcome, it also simultaneously, decreases the surveyable proteome landscape, as non-binding yet relevant proteins are missed. Such techniques are also unsuitable for pure discovery-based approaches as it requires prior knowledge of important proteins. In another study using the visual cortical tissue during the critical period, Dahlhaus *et al.* (2011) measured and identified synaptic proteins that were differentially regulated by developmental age or by altering visual experience. They discovered differentially regulated proteins or complexes of proteins that are either associated with the cytoskeleton, involved in signal transduction or regulate synaptic efficacy (Dahlhaus *et al.* 2011).

Networks provide a powerful means of improving analysis on proteomics data (Goh *et al.* 2011, 2012; Goh and Wong 2013), e.g. expanding the analyzable proteome space by recovering relevant proteins unobserved in the primary screen (Goh *et al.* 2013a). Networks may also be used for dealing with clinical/biological heterogeneity while demonstrating good noise tolerance even at high false discovery rates (Goh *et al.* 2015). Hence, a network-based approach is possibly useful for making better sense of comparative synaptic proteome data.

Despite the surge in neuroepigenomics studies (Satterlee *et al.* 2015), protein arginine methylation is poorly understood and less established compared to their counterparts. Catalyzed by a family of enzymes known as protein arginine methyltranferases (EC 2.1.1), PRMTs catalyze the formation of methylated arginine, which since its discovery, has been implicated in cellular functions such as transcriptional regulation, mRNA processing, nuclear cytoplasmic shuttling, DNA repair, and signal transduction (Bedford and Clarke 2009; Wolf 2009; Yang and Bedford 2013; Jahan and Davie 2015). *Prmt8*, in particular, is brain specific, non-redundant from its familiar homologs and has been described to be important across various stages of neuronal development, e.g. embryonic (Chittka 2010; Lin *et al.* 2013) and postnatal development (Taneda *et al.* 2007; Kousaka *et al.* 2009). Recently, PRMT8 is reported to possess phospholipase activity in the cerebellum (Kim *et al.* 2015) where Purkinje cell dendrite arborization and motor coordination are regulated. Despite these studies, the precise epigenetic mechanisms are not well established. We hypothesize that PRMT8 contributes to the regulation of protein expression within cortical neurons, as well as the synaptic space, thereby influencing synaptic maturation. Since

synaptic proteome profiling has not been done in the context of *Prmt8* perturbation, we study this in the context of two transgenic mouse models ($Prmt8^{+/-}$ and $Prmt8^{-/-}$), using network-based analysis as a means of improving recovering undetected yet relevant proteins, as well as identifying any functionally interesting network modules.

Materials and methods

Animals used

Prmt8 knockout mice ($Prmt8^{tm1a(EUCOMM)Wtsi}$) were obtained from EUCOMM, IKC (European Conditional Mouse Mutagenesis, International Knockout Mouse Consortium) and can be located in the IMPC (International Mouse Phenotyping Consortium) database (www.mousephenotype.org/data/genes/MGI:3043083#section-associations). The transgenic mice were derived from C57BL/6Dnk genetic background. The L1L2_Bact_P vector cassette was inserted upstream of the critical exon(s) on chromosome 6. The cassette consists of a flippase recognition target site, followed by lacZ sequence and a loxP site. This first loxP site is followed by neomycin under the control of the human β-actin promoter, SV40 polyA, a second flippase recognition target site and a second loxP site. A third loxP site is inserted downstream of the targeted exon(s). All experimental mice were maintained on a 12 h light/dark (LD) cycle and had access to food and water *ad libitum*. Common husbandry procedures were used to breed the mice. All animal procedures were approved by the Institutional Animal Care and Use Committee (IACUC) at Biopolis Resource Centre, A*STAR. Mice between the ages of postnatal day, P26-P28 were used for molecular experiments which include iTRAQ, western blotting validation, ChIP, and immunohistochemistry. For behavioral experiments, animals were trained and tested from P26-P27. Experiments were also conducted without gender bias.

Nomenclature

Because of the wide usage of gene and protein databases across our analysis, gene symbols were used as a unifying identifier over International Protein Index (IPI), Uniprot and protein names for consistency and clarity.

Synaptic proteome extraction

Four pairs of visual cortices from wild-type ($Prmt8^{+/+}$), heterozygous ($Prmt8^{+/-}$), and homozygous ($Prmt8^{-/-}$) knockout mice, respectively, were pooled together to obtain sufficient protein (200 μg) for analysis. The synaptic proteome was extracted as previously described in literature (Dahlhaus *et al.* 2011). Briefly, the tissues were homogenized with a motorized pellet pestle (Sigma Aldrich, St. Louis, Missouri, U.S.A.) in buffer containing protease inhibitors (cOmplete, Mini, EDTA-free Protease inhibitor, cat. no. 1183617001; Roche, Basel, Switzerland) until there were no visible cell clumps. Cell debris was carefully removed by a 0.85–1.25 M sucrose-gradient ultracentrifugation. The resulting synaptosomes, the fraction between the two sucrose gradients, were pelleted and lysed by osmotic shock. A second sucrose-gradient ultracentrifugation was performed to isolate and purify the synaptic proteins. Protein concentration was determined using the Prostain Protein Quantification kit (cat. no. 15001; Active Motif, Carlsbad, California, U.S.A) based on manufacturer's guide.

iTRAQ sample preparation, labeling, and tandem LC-MS

iTRAQ is a labeling technique that allows up to eight samples to be simultaneously analyzed (Ross *et al.* 2004). Here, we used the iTRAQ 4-plex labeling kit (Channels 114–116). Synaptic proteins extracted from visual cortices of wild-type ($Prmt8^{+/+}$), *Prmt8* heterozygous mice ($Prmt8^{+/-}$), and *Prmt8* homozygous ($Prmt8^{-/-}$), were separated via sodium dodecyl sulfate–polyacrylamide gel electrophoresis, excised, digested with trypsin, and labeled with iTRAQ tags. The tagged peptides were then separated using Electrostatic Repulsion-Hydrophobic Interaction Chromatography (Alpert 2007) into 20 fractions. Each fraction was analyzed using a QStar Elite LC-MS/MS system (AB Sciex, Framingham, Massachusetts, U.S.A.). Library search was performed using ProteinPilot (Paragon Algorithm, v2.01, AB Sciex.) and the IPI mouse database. Target-decoy database search was used to determine the global false discovery rate, which is set to 1%. Peptide quantitation is determined by absolute tag counts per channel. This is converted to ratios 116/114 ($Prmt8^{-/-}/Prmt8^{+/+}$) and 115/114 ($Prmt8^{+/-}/Prmt8^{+/+}$). Protein expression ratios are calculated from constituent unique peptides by averaging the ratios. The final data matrix contained 2358 proteins.

Differential protein identification

Prior to differential protein identification, we first checked that ratios 116/114 ($Prmt8^{-/-}/Prmt8^{+/+}$) and 115/114 ($Prmt8^{+/-}/Prmt8^{+/+}$) correlated well to each other. Log-conversion followed by z-normalization was performed to ensure that the protein expressions for 116/114 ($Prmt8^{-/-}/Prmt8^{+/+}$) and 115/114 ($Prmt8^{+/-}/Prmt8^{+/+}$), respectively, was normally distributed. An alpha of 5% was defined as the differential cut-off: i.e. proteins with z-scores below −1.96 and above 1.96. To increase confidence in the differential list (given biological and technical variability), we considered the intersection of differential proteins in 116/114 ($Prmt8^{-/-}/Prmt8^{+/+}$) and 115/114 ($Prmt8^{+/-}/Prmt8^{+/+}$).

Overlap analysis

Intersections and overlaps were diagrammatically represented using Venny, a Venn diagram visualizer (Oliveros 2015).

Functional analysis

GO-term functional analysis was performed using Go::TermFinder (Boyle *et al.* 2004). To determine if a GO-term was enriched within a specified list of proteins at a frequency greater than expected by chance, GO::TermFinder calculates a *p*-value (*P*) using the hypergeometric distribution:

$$P = 1 - \sum_{i=0}^{k-1} \frac{\binom{M}{i}\binom{N-M}{n-i}}{\binom{N}{i}}$$

where N is the total number of genes in the reference distribution, M is the number of genes within reference annotated to the GO term, n is the size of the protein list, and k is the number of proteins within annotated to the GO term.

Network analysis

Gene-mania (http://www.genemania.org) is a powerful network visualizer tool, allowing users to determine the functional inter-

connections among their differential protein list as well as implicating additional proteins that are closely associated (Mostafavi *et al.* 2008). Functional interactions include protein-interaction data, pathway, protein and gene expressions, and synthetic lethal relationships.

Gene-Mania boasts a novel approach toward functional annotation based on network edge weights, which was shown to outperform older 'functional assignments based on query gene approaches'. In this approach, for a list of proteins, network weights were assigned based on how well they reproduce GO co-annotation patterns for that organism in the molecular function, biological process, or cellular component hierarchies.

OpenMS/TOPPAS pipeline development

To complement the existing proteomics analysis pipeline, which was provided by the proteomics service facility, and to recover undetected proteins of interest, we built our own proteomics analysis pipeline using OpenMS/TOPP. This is an open source C++ software library developed by several contributors in Germany (FU Berlin and U. Tuebingen) and Switzerland (ETHZ). It provides built-in algorithms covering all aspects of proteomics analysis from spectra processing, *de novo* identification, database search, statistical analysis to protein assembly.

The UniprotKB (release-2013_09/) reviewed protein sequence database was used as the reference library (Apweiler *et al.* 2004). The reverse decoy library was generated using scripts provided within Proteomatic (Specht *et al.* 2011), tagged with the prefix rev_ and concatenated with the original protein sequence library. The requisite phr, psq, and pin files for indexing the database was generated using BLAST (Altschul *et al.* 1990).

Peptide identification was performed using Omssa (Geer *et al.* 2004) and X!Tandem (Bjornson *et al.* 2008) and merged into a single file. A posterior error probability cutoff of 0.7 was used and remaining peptide spectra matches are quantified using the iTRAQAnalyzer module.

In the protein assembly step, the mean of the top three peptides was used as signal intensities for the assembled protein. The channel ratios 116/114 ($Prmt8^{-/-}/Prmt8^{+/+}$) and 115/114 ($Prmt8^{+/-}/Prmt8^{+/+}$) were reconstructed based on these mean signal intensities per protein.

Western blotting analysis

The synaptic fraction was collected from three separate pairs of visual cortices and pooled for western blotting validation using an identical extraction protocol as described above. A total of 10–20 μg were loaded for into each well and concentrations were kept consistent for each protein analyzed. Loading concentrations for Dynein immunoblot were increased to encourage better transfer of protein, because of the inherent difficulties in transferring large molecular weight proteins using a semi-dry transfer system. Synaptic proteins were separated on a 4.5% (wt/vol) polyacrylamide stacking gel, followed by a 5–10% (wt/vol) polyacrylamide resolving gel depending on molecular weight. The proteins were transferred to polyvinylidene difluoride (cat. no. IPFL0010; EMD Millipore, Billerica, Massachusetts, U.S.A.) membranes and were blocked with LI-COR Odyssey® Blocking Buffer (cat. no. 927–4000; LI-COR Bioscience, Lincoln, Nebraska, U.S.A). Subsequently, the membranes were incubated with the appropriate primary antibodies diluted to the recommended concentrations. Excess primary antibody was removed before secondary antibodies were applied to the blots. The membranes were placed onto the LI-COR Odyssey® scanner and processed accordingly.

ChIP and ChIP-qPCR

We first confirmed the specificity of the antibodies by western blot and optimized the antibody amount for ChIP empirically to ensure efficient ChIP. Material from eight pairs of visual cortex was required for each biological replicate. A total of six biological replicates ($n = 6$) and three biological replicates ($n = 3$) were used for wild-type $Prmt8^{+/+}$ and $Prmt8^{-/-}$ samples, respectively. The tissues were fixed with formaldehyde, lysed, and sheared with the Bioruptor® (Diagenode, Denville, New Jersey, U.S.A.) for 15 cycles of 30 s ON/OFF intervals. Samples were pre-cleared and incubated with anti-PRMT8 antibody or mouse IgG controls at 4°C overnight. Immune-complexes were pulled down with magnetic beads, reverse cross-linked, and purified with phenol-chloroform.

The sheared chromatin was then used to analyse relative enrichment of *Tenascin-R* (*Tnr*) promoter regions (Putthoff *et al.* 2003). Four sets of RT-qPCR primers were designed to cover the entire promoter region. They are: *Tnr* promoter region 1 (P1) forward primer 5′-CCATCAGGACTGGGACTGTTT-3′; *Tnr* promoter region 1 (P1) reverse primer 5′-CCTTCTACAAGTAGCCCCCTA-3′; *Tnr* promoter region 2 (P2) forward primer 5′-ACAGCTTAAAAA-TATGCTGCTGAA-3′; *Tnr* promoter region 2 (P2) reverse primer 5′-GTCTCTGCGTGTTGAGCCA-3′; *Tnr* promoter region 3 (P3) forward primer 5′-GCAGCCTCAGAGACAGGGAA-3′; *Tnr* promoter region 3 (P3) reverse primer 5′-AAACAGCAGCTGG TAGGTCT-3′; *Tnr* promoter region 4 (P4) forward primer 5′-GTGAAGCCTTCTCTCTGCCTC-3′; *Tnr* promoter region 4 (P4) reverse primer 5′-AGCTAGAGCAGCTTCCAAAGCA-3′; chromosome 8 untranscribed region forward primer 5′-GGGTCCCCAGAG-GAACACA-3′; chromosome 8 untranscribed region reverse primer 5′-TGACCTCACTGCAGACAAGGA-3′. Raw Ct values were extrapolated and the Ct values for input samples were adjusted for dilution factor. Data were represented as fold enrichment and finally normalized to IgG.

RNA extraction and Real-time quantitative PCR

Total RNA was isolated from independent pairs of snap frozen visual cortical tissue using RNeasy® Lipid Tissue Mini Kit (cat. no. 74804; Qiagen, Venlo, Netherlands.). mRNA was converted to cDNA using the High Capacity cDNA Reverse Transcription Kit (cat. no. 4368813; Applied Biosystems Inc., Foster City, California, U.S.A). Real-time qPCR was conducted and detected using SYBR® Green technology (Applied Biosystems Inc.) on the FAST7900HT (Applied Biosystems Inc.) machine. Primers used include: *Tnr* forward primer 5′-AGACCTGGCTCGCGCTACGA-3′, *Tnr* reverse primer 5′-GTGCGGGAACCCACTCGCAA-3′; *β-actin* forward primer 5′-CCACTGCCGCATCCTCTTCC-3′; *β-actin* reverse primer 5′-CTCGTTGCCAATAGTGATGACCTG-3′; *eukaryotic 18S rRNA* forward primer 5′-GCTTCCTTACCTGGTTGATCCTG-3′; *eukaryotic 18S rRNA* reverse primer 5′-TGATTTAATGAGC-CATTCGCAG-3′. Delta CT values were calculated with two housekeeping genes: *eukaryotic 18S rRNA* and *β -actin*. The final fold-change is the average of the two values.

Immunohistochemistry

Brain tissues were fixed with 4% (wt/vol) paraformaldehyde extracted carefully, post-fixed and cryoprotected in sucrose overnight. Perfused brains were sectioned at 40 μm thickness with a

cryostat. The sections were blocked with appropriate antisera and detected with appropriate dilutions of primary and secondary antibodies (please refer to next section). 4',6-diamidino-2-phenylindole (DAPI, 1 mg/mL) was used to counter-stain the nuclei of cells. Immunofluorescence imaging was performed with a confocal laser-scanning microscope (Nikon A1. Nikon Instruments

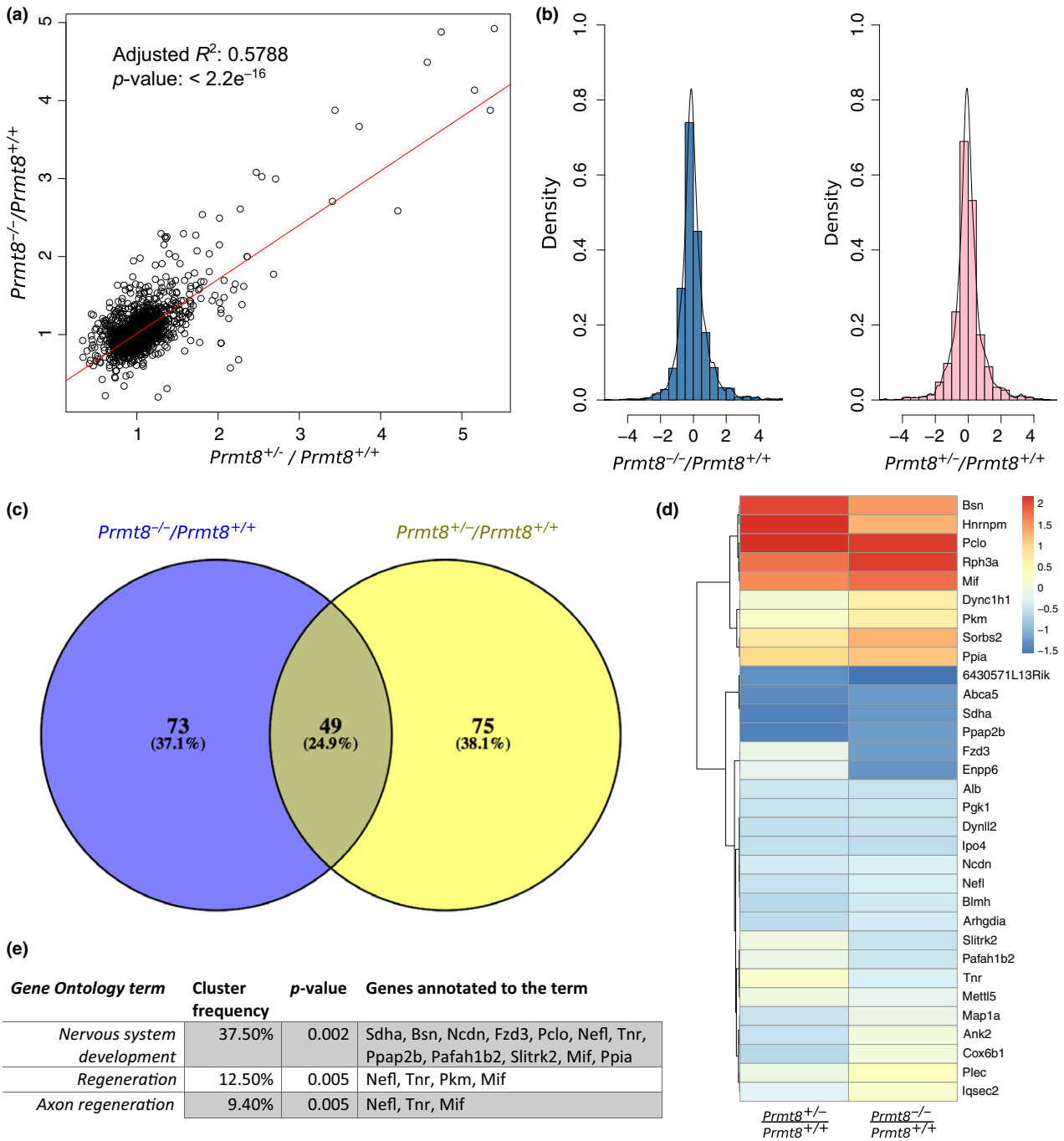

(e)

Gene Ontology term	Cluster frequency	*p*-value	Genes annotated to the term
Nervous system development	37.50%	0.002	Sdha, Bsn, Ncdn, Fzd3, Pclo, Nefl, Tnr, Ppap2b, Pafah1b2, Slitrk2, Mif, Ppia
Regeneration	12.50%	0.005	Nefl, Tnr, Pkm, Mif
Axon regeneration	9.40%	0.005	Nefl, Tnr, Mif

Fig. 1 Protein-based expressions showed good correlations between the partial and complete *Prmt8* knockouts but limited overlaps between their respective differential genes, although these were nonetheless enriched for neurological processes. (a) The expression distributions for each isobaric tag (116 for homozygous knockout, –/–; 115 for heterozygous, +/– & 114 for wild type, +/+) were generally well-correlated and (b) are normally distributed. Only proteins with values beyond ± 1.96 were considered differentially expressed as determined by their z-normalized expression values. (c) Venn diagram showed limited overlaps (49 genes, 25% agreement) between heterozygous (+/–) and homozygous (–/–) *Prmt8* knockouts. (d) Clustering of 49 genes revealed four major groups based on expressional intensity changes but most were down-regulated. (e) Functional analysis based on GO-terms pointed strongly toward enrichment of GO-terms associated with nervous system development, in particular, axon regeneration.

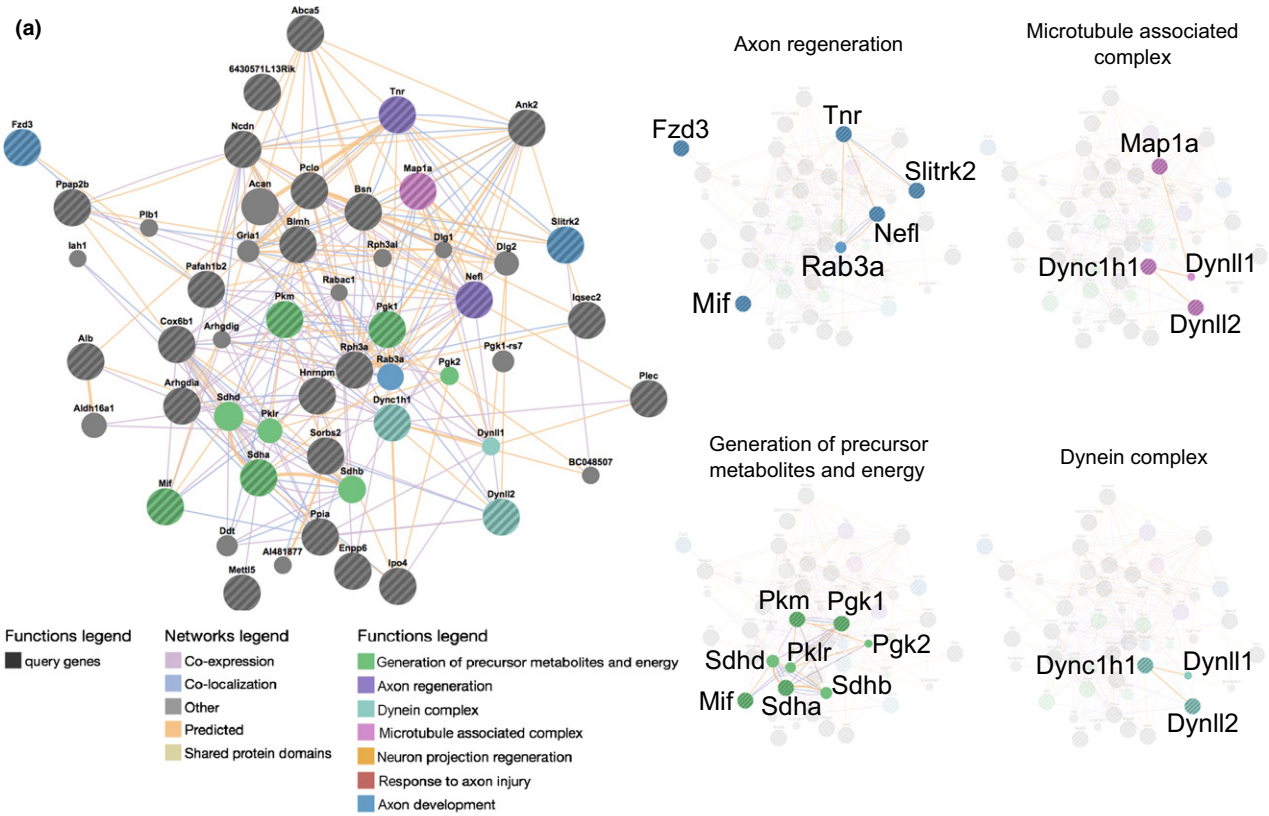

(b)

Gene Ontology term	Coverage	FDR	Genes annotated to the term
Generation of precursor metabolites and energy	8/196	4.66e-4	Mif, Pgk1, Pgk2, Pkm, Pklr, Sdha, Sdhb, Sdhd
Axon regeneration	3/21	3.68e-2	Nefl, Slitrk2, Tnr
Dynein complex	3/23	3.84e-2	Dync1h1, Dynll1, Dynll2
Microtubule-associated complex	4/69	3.84e-2	Dync1h1, Dynll1, Dynll2, Map1a
Neuron projection regeneration	3/28	6.4e-2	Nefl, Slitrk2, Tnr
Responseto axon injury	3/31	7.64e-2	Nefl, Slitrk2, Tnr
Axon development	6/288	8.32e-2	Fzd3, Mif, Nefl, Rab3a, Slitrk2, Tnr

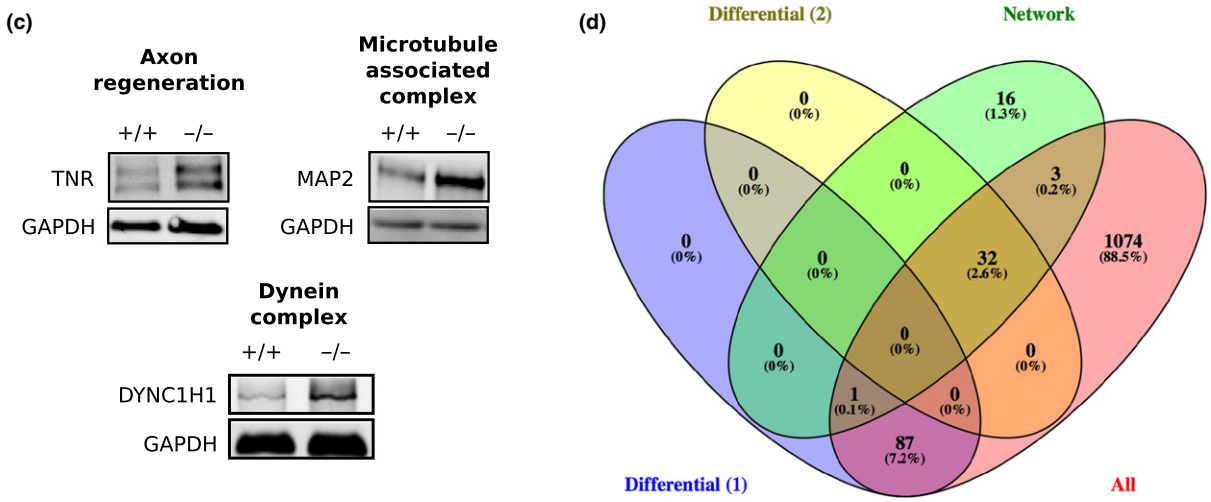

Fig. 2 The disrupted functional network induced by *Prmt8* knockout was enriched for relevant neuronal processes, in particular dendritic development. (a) The common differential genes from both heterozygous (*Prmt8*$^{+/-}$) and homozygous (*Prmt8*$^{-/-}$) *Prmt8* knockouts (32 mappable to gene names out of the original 49) induced a highly interconnected network, further implicating an addition 20 proteins excluded during the preliminary proteomics screen. This network, induced by the differential proteins from the complete reference network, may be further subdivided into domains based on functionality, which included axon regenration, microtubule association and formation of dynein complexes. (b) Table denoting enriched GO terms, coverage (ratio of differential proteins over all proteins mapped to particular term), associated false discovery rates (FDR) and differential gene membership within each network. (c) Representative immunoblots of one representative protein from each functional group (except generation of metabolites and energy) demonstrated increased expression in *Prmt8*$^{-/-}$ mice compared to *Prmt8*$^{+/+}$ (tenascin-R, TNR: $n = 5$; MAP2: $n = 3$; and DYNC1H1: $n = 3$). (d) Although the 32 differential proteins; Differential (2), or proteins that were supported by both knockouts, were associated with relevant functionalites, they were not easily observed or recovered in the proteomics screen. Of the 20 network implicated proteins, only 1 was recoverable given the set of non-overlapping differential proteins supported by either knockout; Differential (1). While low, the maximal recovery rate is not 1/20 but rather 1/4 as only four implicated proteins were potentially recoverable (All). Since most implicated proteins were not observed in the preliminary spectra analysis, a wider search on protein spectra may be required.

Inc., Melville, New York, U.S.A). Images settings were optimized with the control wild-type sections and kept constant.

Antibodies used

Primary antibodies used include anti-Dynein antibody (DYNC1H1, cat. no. sc-9115, 1 : 200 dilution for western blotting; Santa Cruz Biotechnology, Inc., Dallas, Texas, U.S.A.); anti-GAPDH antibody (GAPDH, cat. no. G8795, 1 : 10 000 dilution for western blotting; Sigma Aldrich); rabbit IgG antibody (cat. no. 12–370, 4 μg for ChIP; EMD Millipore); anti-MAP2 antibody (MAP2, cat. no. MAB3418, 1 : 1000 dilution for western blotting; EMD Millipore); anti-PRMT8 antibody (cat. no. sc-130853, 1 : 50 for immunostaining, Santa Cruz Biotechnology, Inc.; cat. no. ab73686; 1 : 250 dilution for western blotting and 4 μg for ChIP; Abcam, Cambridge, United Kingdom.); anti-parvalbumin antibody (PV, cat. No. PV235 or PV28, 1 : 500 for immunostaining; Swant Inc., Marly, Switzerland.); anti-tenascin-R antibody (TNR, cat. no. sc-136098, 1 : 200 dilution for western blotting; Santa Cruz Biotechnology, Inc.); anti-vesicular GABA transporter antibody (VGAT, cat. no. AB5062P, 1 : 200 dilution for immunostaining; EMD Millipore); Biotinylated *Wisteria floribunda* agglutinin lectin (cat. no. B1355, 1 : 100 for immunostaining; Vector Laboratories, Burlingame, CA, USA). Secondary antibodies used include a range of Alexa Fluor® dyes for different excitation wavelengths (1 : 200 for immunostaining; Molecular Probes, Eugene, OR, USA) or IRDye 800CW antibodies (1 : 3000 for immunoblotting; LI-COR Bioscience).

Golgi-cox staining and 3D reconstruction

Brain from P28 wild-type and *Prmt8* knockout mice ($n = 5$ each) were fixed, extracted, post-fixed, and processed in solutions from Rapid GolgiStain™ kit (FD Neurotechnologies, Inc., Columbia, Maryland, U.S.A) according to the manufacturer's protocol. Impregnated brain tissues were sectioned at 150 μm thickness with a cryostat, stained and dehydrated according to the manufacturer's protocol.

Neuron reconstruction and quantitative analyses were conducted by MicroBrightField Labs and was blind to sample genotype. A total of nine neurons were constructed – four neurons (sampled from $n = 5$ wild-type *Prmt8*$^{+/+}$ mice) and five neurons (sampled from $n = 5$ *Prmt8*$^{-/-}$ mice). Neurons in the visual cortex selected for reconstruction were uniformly impregnated, with the soma positioned within the middle of the histological section. Chosen cells demonstrated distinct spines and dendritic arbors with minimal breaks or staining irregularities. Neurons were reconstructed using a modified light microscope (Zeiss AxioImager Z1. Carl Zeiss AG, Oberkochen, Germany). under 100× oil (1.4 numerical aperture; Plan-Apochromat) controlled by Neurolucida software (v.10.5; MBF Bioscience, Williston, VT, USA). The microscope system had an internal Z motor, a motorized specimen stage (Ludl Electronics, Hawthorne, NY, USA), external focus encoder (Heidenhain, Schaumburg, IL, USA), and a CCD monochrome video camera (mRm; Zeiss). Neurons were traced in their entirety, matching dendritic diameter and location of dendritic spines. The soma was traced at its widest point in the two-dimensional plane to estimate the cross-sectional area. Neurons that displayed breakages in dendrites were not included in final analysis.

Fluorescent imaging of perineuronal nets

Fluorescence imaging for synapse number was conducted as previously described (Ippolito and Eroglu 2010). For perineuronal nets (PNNs) intensity analysis, 30–60 z-stack images were imaged at 0.3 μm intervals to cover the entire soma. Maximum intensity projection was performed to reveal the entire cell body. Fluorescence intensity of the PNNs around the soma is measured using the ImageJ (Schneider *et al.* 2012) software. Corrected total cell fluorescence (CTCF) was calculated using this formula (McCloy *et al.* 2014):

$$\text{CTCF} = \text{integrated density} - (\text{area of ROI} \times \text{mean fluorescence of background})$$

Images settings were optimized with the control wild-type sections and kept constant for all other acquisitions.

Visual water task

The visual water task is a visual discrimination task based on reinforcement learning (Prusky *et al.* 2000; Prusky and Douglas 2004). The task consists of a trapezoidal aluminum tank (183 cm long × 82 cm wide × 73 cm high) with two screens depicting vertical striations or an equiluminant gray stimulus at the wider end (Figure S2a). Animals were initially pre-trained to associate getting to a solid substrate (hidden platform) by swimming toward a low spatial frequency vertically striated screen (positive stimuli). Once the animals have grasped the reward concept, they underwent training and testing phases (Figure S2b) where their abilities are shaped to distinguish between the vertical gratings and the

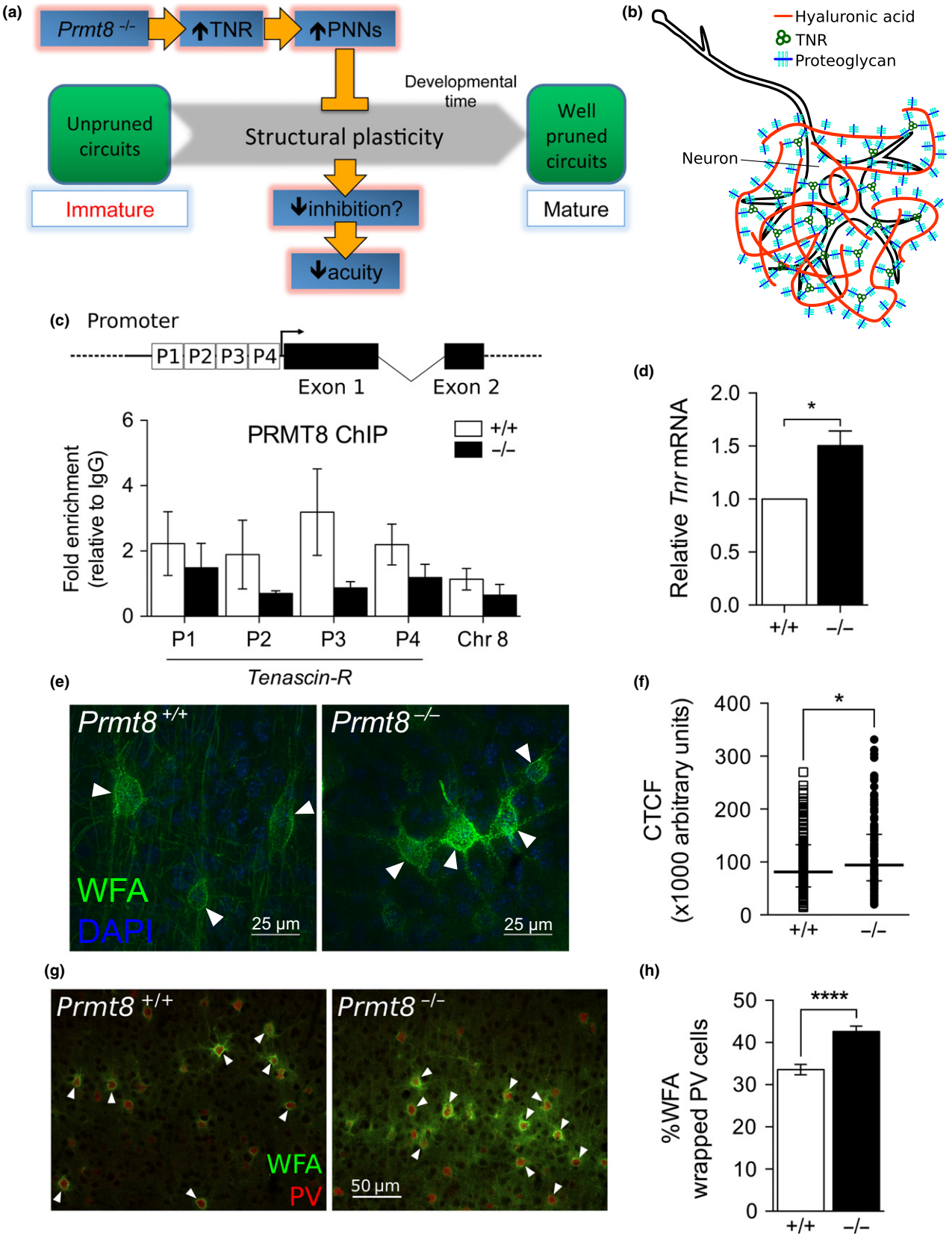
(a)
Prmt8 -/-
↑TNR
↑PNNs
Developmental time
Unpruned circuits
Structural plasticity
Well pruned circuits
Immature
↓inhibition?
Mature
↓acuity
(b)
Hyaluronic acid
TNR
Proteoglycan
Neuron
(c) Promoter
P1 P2 P3 P4
Exon 1
Exon 2
PRMT8 ChIP
+/+
–/–
Fold enrichment (relative to IgG)
P1 P2 P3 P4 Chr 8
Tenascin-R
(d)
Relative Tnr mRNA
+/+ –/–
(e)
Prmt8 +/+
Prmt8 –/–
WFA
DAPI
25 µm
(f)
CTCF (x1000 arbitrary units)
+/+ –/–
(g)
Prmt8 +/+
Prmt8 –/–
WFA
PV
50 µm
(h)
%WFA wrapped PV cells
+/+ –/–

Fig. 3 Knockout of *Prmt8* limited structural plasticity of the visual cortex via increased perineuronal net (PNN) formation. (a) Proposed model of aberrant neuronal development of the visual cortex in *Prmt8* knockout mice. Experience-dependent pruning of cortical circuits over development (gray arrow) provided the necessary biological mechanisms to make circuits fully functional. Increased PNN formation in the visual cortex of *Prmt8* knockout model prevented the pruning and maturation of excitatory synaptic connections (orange arrows) by reducing inhibitory modulation of excitatory neurons through limiting structural plasticity. Reduction of inhibitory puncta may possibly lead to a drop in overall inhibition in the visual cortex. (b) Tenascin-R (TNR) is a crucial component of special brain extracellular matrix structures called PNNs, which form around parvalbumin inhibitory interneurons. Trimeric TNR (green circles) acts as a linker protein between hyaluronic acid (red line) and proteoglycans (blue structure) to form an organized mesh-like structure (Lau *et al.* 2013; Morawski *et al.* 2014; Mouw *et al.* 2014). (c) ChIP analysis indicated that PRMT8 was enriched at *Tenascin-r (Tnr)* promoter regions (top schematic). Immunoprecipitation (bottom plot) of wild-type $Prmt8^{+/+}$ visual cortices (open bars, $n = 6$) with PRMT8 antibody showed increased PRMT8 association with chromatin at the promoter region of *Tnr* ($p = 0.01$, one-sample *t*-test,) compared to the untranscribed region on chromosome 8. Removal of *Prmt8* abolished PRMT8 enrichment levels (closed bars, $n = 6$) to levels comparable to control IgG antibody levels. (d) *Tnr* transcript levels were 1.5 fold higher compared to wild-type levels ($p \leq 0.05$, $n = 3$ each, unpaired Student's *t*-test). (e) Representative photomicrographs of PNNs (arrows) in binocular zone of the visual cortex from wild-type $Prmt8^{+/+}$ (left) and $Prmt8^{-/-}$ mice (right) immunostained with biotinylated *Wisteria floribunda agglutinin* (WFA) and DAPI. WFA is routinely used as a broad marker in the detection of PNNs. (f) Density of PNNs, as measured by CTCF, was increased around neurons of $Prmt8^{-/-}$ mice ($p \leq 0.05$, $n = 3$ each, Mann–Whitney *U*-test). Data were represented as median CTCF. (g) Representative photomicrographs of the binocular zone of the visual cortex from wild-type $Prmt8^{+/+}$ (left) and $Prmt8^{-/-}$ (right) mice immunostained with biotinylated WFA and parvalbumin (PV). Arrows indicate PV interneurons wrapped by PNNs. (h) In addition to increased density of PNNs, approximately 10% more PV-positive interneurons were wrapped by PNNs in $Prmt8^{-/-}$ mice than in wild-type $Prmt8^{+/+}$ mice ($p \leq 0.0001$, $n = 3$ each, unpaired Student's *t*-test). Data were represented as mean ± SEM. $*p \leq 0.05$, $****p \leq 0.0001$.

equiluminant gray stimulus at a short distance (training) and at a longer distance (testing). The position of the grating and the platform was alternated in a pseudorandom sequence over the training and test trials. Once 70% or greater accuracy was achieved in a series of 10 trials, the spatial frequency of the grating increases until trial performance falls below 70% accuracy. The maximum visual acuity was measured with three consecutive passes of the highest spatial frequency. The mice were trained from postnatal day P28 for 2–3 months (P90-P120) to obtain the discrimination threshold.

Statistical analysis

Datasets were tested for normality using the Kolmogorov–Smirnov goodness-of-fit test. Data with parametric distributions were expressed as mean ± SEM and statistical analyses were performed with the Student's *t*-test. Data with non-parametric distribution (e.g. Fig. 3f) were expressed as median ± SD and statistical analysis were performed with the Mann–Whitney *U*-test.

Results

Despite limited overlap, common differential proteins were enriched for neuronal functionalities

It was well known that data-dependent acquisition-based proteomics had limited consistency because of the semi-stochastic manner in which precursor ions were selected for fragmentation in MS/MS space (Goh and Wong 2014). Despite this, $Prmt8^{-/-}/Prmt8^{+/+}$ and $Prmt8^{+/-}/Prmt8^{+/+}$ were generally correlated (Fig. 1a). Following log-conversion and z-transformation, the protein expression distributions for $Prmt8^{-/-}/Prmt8^{+/+}$ and $Prmt8^{+/-}/Prmt8^{+/+}$ were normally distributed (Fig. 1b) and therefore, we introduced an alpha of 5%, i.e. proteins with z-scores below −1.96 and above 1.96 were considered differentially expressed.

Only 25% (49 proteins) of the differential proteins between $Prmt8^{+/-}/Prmt8^{+/+}$ and $Prmt8^{-/-}/Prmt8^{+/+}$ were shared (Fig. 1c) while 75% (148 proteins) lied in the complement. The 49 IPI ids were mapped to 32 proteins with gene symbols. Hierarchical clustering based on z-normalized protein expressions (Euclidean distance, Ward's linkage) revealed most of these were down-regulated (Fig. 1d). Functional analysis based on Gene Ontology (GO)-terms pointed revealed strong association with nervous system development, especially, axon regeneration (Fig. 1e).

Analysis of differential networks did not strongly recover complement proteins

Networks are powerful means of recovering undetected proteins (Goh *et al.* 2013a). Given many different networks exist (e.g. protein interaction networks, expression correlational), we used the integrated platform, GeneMania (Mostafavi *et al.* 2008; Montojo *et al.* 2014) with the 32 gene symbols as seeds. This returned a tightly inter-connected induced network comprising 52 genes (20 implicated genes + 32 gene symbols corresponding to the differential proteins) (Fig. 2a). The induced network was enriched for neurological functionalities (similar to Fig. 1e), but more extensive. Moreover, additional functional terms were implicated, such as microtubule-associated complex, energy metabolism, and dynein complexes (Fig. 2a and b). Each of these additional functionalities were attributable to specific locations in the induced network. We checked the expressions of each subnet indirectly via immunoblotting of a representative protein in each functional subnet (Fig. 2c): TNR (axon regeneration, $n = 5$), MAP2 (microtubule-associated complex, $n = 3$), and DYNC1H1 (dynein complex, $n = 3$) were over-expressed in *Prmt8* knockout mice compared to wild type.

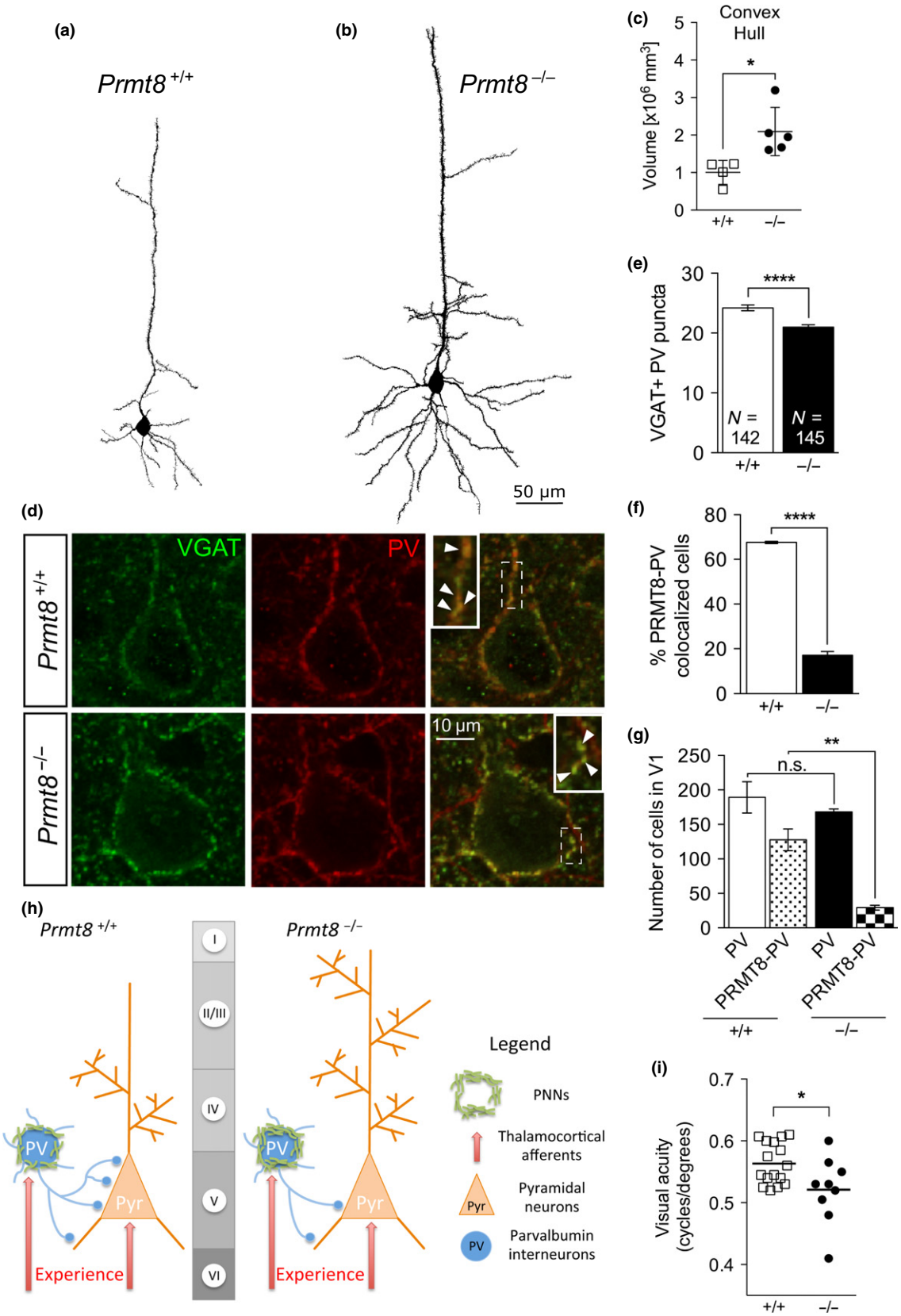
(a)
Prmt8 +/+
(b)
Prmt8 −/−
50 µm
(c)
Convex Hull
Volume [x10^6 mm^3]
*
+/+
−/−
(e)
VGAT+ PV puncta
****
N = 142
N = 145
(d)
VGAT
PV
Prmt8 +/+
Prmt8 −/−
10 µm
(f)
% PRMT8-PV colocalized cells
****
(g)
Number of cells in V1
n.s.
**
PV
PRMT8-PV
(h)
Prmt8 +/+
Prmt8 −/−
I
II/III
IV
V
VI
PV
Pyr
Experience
Legend
PNNs
Thalamocortical afferents
Pyramidal neurons
Parvalbumin interneurons
(i)
Visual acuity (cycles/degrees)
*

Fig. 4 Visual circuits of *Prmt8* knockout mice were not fully pruned and these mice suffered from lower visual acuity. Representative reconstruction of Golgi-Cox stained (a) wild-type *Prmt8*$^{+/+}$ neuron and (b) *Prmt8*$^{-/-}$ neuron. (c) Convex hull analysis revealed that neurons (filled circles, $n = 5$) in the visual cortex of *Prmt8*$^{-/-}$ mice had more branching events than wild-type neurons (open squares, $n = 4$), which were more compact ($p \leq 0.05$, unpaired Student's *t*-test). (d) Representative photomicrographs of coronal sections of the primary visual cortex from P27 wild-type *Prmt8*$^{+/+}$ mice (top) and *Prmt8*$^{-/-}$ mice (bottom) stained with VGAT (green) and PV (red). Colocalized puncta (arrows in inset) represented inhibitory synapses. (e) Wild-type *Prmt8*$^{+/+}$ neurons ($N = 142$ somas) have more VGAT+/PV+ inhibitory puncta than neurons in *Prmt8*$^{-/-}$ mice ($p \leq 0.0001$, $N = 145$ somas, unpaired Student's *t*-test). (f) PRMT8 was localized in PV+ neurons ($n = 3$, $p \leq 0.0001$, unpaired student *t*-test). (g) Despite reduction of PV-PRMT8 co-localization events ($n = 3$, $p \leq 0.01$, unpaired Student's *t*-test), the number of PV neurons was not reduced in *Prmt8* knockout. (h) Schematic representation of local cortical circuit arrangement involving an excitatory (Pyr; pyramidal) and an inhibitory (PV; parvalbumin) neuron. In wild-type *Prmt8*$^{+/+}$ cortex (left), experience sculpts excitatory circuit connections modulated by inhibitory neurons before consolidation of feedforward inhibitory connections by perineuronal nets. In *Prmt8*$^{-/-}$ cortex (right), formation of excess perineuronal nets (PNNs) restricted structural plasticity of inhibitory neurons, preventing the establishment of inhibitory connections for pruning and maturation of visual cortical circuitry. The layers of the cortex are represented by the gray bar with Roman numerals. (i) At 70% threshold, visual acuity was lower in *Prmt8*$^{-/-}$ mutants ($n = 9$, unpaired Student's *t*-test, $p \leq 0.05$) than wild-type *Prmt8*$^{+/+}$ mice ($n = 16$) when measured by the visual water task. All data were represented as mean ± SEM. $^{*}p \leq 0.05$, $^{**}p \leq 0.01$ $^{****}p \leq 0.0001$.

Earlier, we identified 32 common differential proteins (mappable to gene symbols from 49 IPI ids) while 88 (mappable to gene symbols from the 148 IPI ids) are unique to either *Prmt8*$^{-/-}$/*Prmt8*$^{+/+}$ and *Prmt8*$^{+/-}$/*Prmt8*$^{+/+}$ (Fig. 1c). The large non-overlapping components could be as a result of biological variation against a backdrop of small sample size. Regardless, we wished to know if the non-overlapping components were associated in the same induced network.

In Fig. 2(d), 'Differential(1)' referred to differential proteins that lied in the complement (supported by either complete or partial PRMT8 knockout), 'Differential(2)' for differential proteins supported by either knockout, 'Network' referred to the 52 (32 + 20) proteins within the induced network while 'All' included all the proteins identified in the proteomics screen mappable to gene symbol (1197 proteins). It appeared that the induced network performed very badly in recovery: Only 1 complement protein was recovered, leaving 87 unaccounted for. This was unsurprising considering the maximal number of recoverable proteins: To understand this, we needed to consider overlaps with all detectable proteins ('All' vs. 'Network'). Only three additional proteins were potentially recoverable because of abysmal overlap between 'All' and 'Network'. Given a maximal of 1 + 3 = 4 potentially recoverable proteins, we actually had a recovery rate of 25% (1 out of 4).

Reanalysis using a second proteomics pipeline improved recovery but also revealed inconsistency between different library search engines

Since *Prmt8* was not initially observed, and we had poor recovery of the complement differential proteins, we constructed a second analytical pipeline based on OpenMS/TOPPAS integrating two other search engines, X!Tandem and OMSSA (see Materials and Methods). The OpenMS/TOPPAS pipeline was shown in Figure S1a and we used a rather loose posterior error probability of 0.7 while requiring reported proteins to have at least two unique peptides. We detected and confirmed *Prmt8* as differentially underexpressed (Figure S1d).

Given less stringent statistical criteria, and more extensive search results derived from additional library search algorithms and larger reference protein database, 7172 proteins were observable (Figure S1b 'UniPROT'). This comprised ~ 70% of proteins identified in the original screen (Figure S1b 'All'). 'Differential(2)' and 'Network' referred to intersecting differential proteins and proteins implicated in the induced network, respectively (c.f. Fig. 2c).

Although more proteins were observed, four out of the original 32 intersecting differential proteins were lost. We recovered 10 out of 20 additional proteins implicated by the induced network. Combined with the original screen, we can now account for 12/20 implicated proteins (Figure S1c).

By expanding the observable proteins, we increased our recovery of the induced network, and were able to examine in closer detail, the expression of its individual components. Expansion of the induced network recovered more biologically coherent functionalities, and also enhanced molecular characterization of the *Prmt8* knockout.

Knockout of *Prmt8* causes perineuronal nets to form aberrantly

Using the predictions from both the proteomic and network analysis, we propose that *Prmt8* is an important epigenetic regulator of proteins, such as TNR, that are involved in regulation of structural plasticity required for proper visual development (Fig. 3a). TNR is a crucial linker protein (Morawski *et al.* 2014; Mouw *et al.* 2014) in the mesh-like structure known as perineuronal nets (PNNs; Fig. 3b) that stabilize and restrict plasticity. Chromatin immunoprecipitation (ChIP; Fig. 3c) of wild-type *Prmt8*$^{+/+}$ visual cortices showed enrichment of *Tenascin-R* gene promoter regions (P1: 2.22 fold enrichment ± 0.98; P2: 1.88 fold ± 1.05; P3: 3.18 fold ± 1.32; P4: 2.19 fold ± 0.63, $p = 0.01$, $n = 6$ each) compared to an untranscribed region (Chr 8: 1.13

fold ± 0.33, $n = 6$), whereas, a similar experiment on chromatin from *Prmt8*$^{-/-}$ visual cortices abolished this enrichment (closed bars. P1: 1.48 fold enrichment ± 0.98; P2: 0.66 fold ± 0.08; P3: 1.01 fold ± 0.16; P4: 1.36 fold ± 0.36, $p = 0.22$ $n = 6$ each). *Tnr* transcript levels were increased in the visual cortex of *Prmt8*$^{-/-}$ mice by 1.5 fold ($p = 0.02$, $n = 3$) compared to wild-type *Prmt8*$^{+/+}$ (Fig. 3d). These results suggest that PRMT8 regulates expression of *Tnr* through promoter regions. Since the appearance of PNNs marks the termination of plastic periods during neurodevelopment (Wang and Fawcett 2012), we thought that increased expression of TNR will increase PNN formation and decrease neuroplasticity. To investigate, we immunostained visual cortical tissues with biotinylated *Wisteria floribunda* agglutinin, a plant lectin that binds to carbohydrate groups within PNNs (Fig. 3e). PNNs are about 9% denser within the visual cortex of the *Prmt8*$^{-/-}$ mutants (Fig. 3f. $n = 3$, $N = 95$, 103765 AU, $p = 0.02$) than in the wild-type *Prmt8*$^{+/+}$ ($n = 3$, $N = 111$, 94310 AU). Since PNNs form selectively around parvalbumin (PV) interneurons (Morris and Henderson 2000), we sought to understand if denser PNNs results in PNNs wrapping around more PV interneurons. In the *Prmt8*$^{-/-}$ visual cortex, 10% more PV interneurons were wrapped in PNNs (Fig. 3g and h; 33.58 ± 1.23%, $p < 0.0001$, $n = 3$) than in the wild-type *Prmt8*$^{+/+}$ cortex (42.60 ± 1.31%, $n = 3$).

Previous studies have shown that synaptic plasticity will be affected if PNNs and its components form poorly or incompletely (Zhou *et al.* 2001; Brakebusch *et al.* 2002; Carulli *et al.* 2010; Morawski *et al.* 2014). Similarly, to determine if increased formation of PNNs affected dendritic morphology in V1, neurons from wild-type *Prmt8*$^{+/+}$ mice (Fig. 4a) were compared to age-matched *Prmt8*$^{-/-}$ mutants (Fig. 4b) using Golgi-Cox staining. A two-fold overall increase in volumetric complexity in *Prmt8*$^{-/-}$ neurons compared to the wild-type neurons of the same age (Fig. 4c) (+/+: 1.0 ± 0.16; −/−: 2.094 ± 0.29, $p = 0.02$) was observed. Since PV interneurons provide feedforward inhibition by exerting control on pyramidal neurons, puncta counting analysis was conducted to determine if modulatory PV synaptic connections are affected by *Prmt8* removal. Perisomatic VGAT-positive PV puncta were reduced in *Prmt8*$^{-/-}$ mutants compared to wild type (Fig. 4d and e) (+/+: 24.21 ± 0.49, $n = 3$, $N = 142$; −/−: 20.99 ± 0.39, $p < 0.0001$, $n = 3$, $N = 145$). Immunofluorescence analysis indicated that PRMT8 colocalized in PV+ neurons (Fig. 4f) (*Prmt8*$^{+/+}$: 67.6 ± 0.52%, $n = 3$; *Prmt8*$^{-/-}$: 17.09 ± 1.65%, $p \leq 0.0001$, $n = 3$) and ruled out the possibility that PRMT8 removal will significantly reduce PV+ cell numbers (Fig. 4g) (*Prmt8*$^{+/+}$ PV: 189.3 cells ± 22.67 vs. *Prmt8*$^{-/-}$ PV: 168.3 cells ± 4.10, $p = 0.41$, $n = 3$). These observations suggest that pyramidal neurons in the cortex of *Prmt8*$^{-/-}$ knockout mice receive lesser perisomatic inhibitory connections and may be less developed because of physical restraints set in placed by increased PNNs (Fig. 4h). Despite this, *Prmt8*$^{-/-}$ mice developed normally and did not display any observable deficit, as previously described (Kim *et al.* 2015). However, since inhibition is crucial for the development of the visual cortex (Hensch *et al.* 1998; Fagiolini and Hensch 2000; Prusky and Douglas 2003), we sought to test whether removal of *Prmt8* affected visual acuity. In order to test visual performance, the visual water task (ACUMEN, Cerebral Mechanics Inc) (Prusky *et al.* 2000, 2008; Prusky and Douglas 2004) was used as a measurement of both visual discrimination and acuity (Figure S2a and b). Visual acuity was reduced in the *Prmt8*$^{-/-}$ knockout mice by 8.8% (Fig. 4i) (+/+: 0.56 cyc/deg ± 0.01; −/−: 0.52 cyc/deg ± 0.02, $p = 0.02$).

Discussion

In this study, we have identified and characterized the proteomic changes because of *Prmt8* ablation and its role in the developing visual cortex. Removal or disruption to *Prmt8* via a transgenic mouse model perturbs proteins that are functionally important for axonal or dendritic development. This negatively influenced the development of the visual cortical circuits, as well as the visual performance of the animal.

Although *Prmt8* was not initially detected in our preliminary proteomics analysis (Fig. 1), we have proven the reliability and accuracy of our proteomic screen in the secondary screen (Fig. 2 and Figure S1). From the overlap of 49 differential genes from both *Prmt8* homozygous and heterozygous mutants, 32 mappable genes were clustered into four functional subnets, which are associated with the development of the nervous system. The neurological functions associated with the functional subnets induced by the set of 32 differential genes were in agreement with our expectation that PRMT8 might be an important player in regulating neurodevelopment and/or synaptogenesis during development of the visual cortex. Moreover, enriched GO terms point toward functionalities involving neurite formation and development.

TNR was identified by our first screen of the synaptic proteome. Similar to the other proteins identified, TNR is implicated in neurite development, cell adhesion, and movement (Pesheva and Probstmeier 2000). Interestingly, TNR is only immunohistologically detected from postnatal day 21 in the visual cortex (Brückner *et al.* 2000). This coincides with the developmental expression of *Prmt8* (Kousaka *et al.* 2009), as well as the onset of the critical period of the visual cortex (Hensch 2004). Evidence from ChIP data (Fig. 3c) showed that PRMT8 binds to *Tnr* at its promoter region. Knockout of PRMT8 increased transcript levels of *Tnr* in the visual cortex, suggesting that PRMT8 may act as a molecular brake. However, it is not clear if PRMT8 acts on its putative histone H4 arginine 3 asymmetric methylated mark (H4R3me2a) to regulate the transcriptional machinery. TNR is an integral extracellular matrix component of PNNs, acting as a cross-linker between

hyaluronan and chondroitin sulfate proteoglycan (CPSGs), aggrecan (Lundell *et al.* 2004) (Fig. 3b). Together, these three molecules (hyaluronan, CPSG, and TNR) form the three major components of the perineuronal net. TNR is suggested to be more important than CPSGs because nets in *Tnr*-deficient mice fail to aggregate properly (Weber *et al.* 1999) but CPSG-deficient mice still form normal nets (Zhou *et al.* 2001; Brakebusch *et al.* 2002). Besides protecting the neurons from extracellular chemicals or agents, PNNs also limit synaptic plasticity by stabilizing the functional, matured neuronal connections. This was demonstrated by enzymatic digestion of the PNNs, which reverted adult mice back to the juvenile state of ocular dominance plasticity (Pizzorusso *et al.* 2002). In addition, aggrecan (Acan, Figure S1d), another component of PNN, was recovered in our second proteomics pipeline (Figure S1b), further supporting our observation that knockout of *Prmt8* does affect formation of these nets. TNR and Acan are reported as crucial contributors to the formation and stabilization of PNNs (Morawski *et al.* 2014). Similar to TNR, Acan has been implicated as a molecular controller of structural plasticity in the neocortex. A previous study demonstrated that Acan expression correlates with a decline in plasticity in the visual cortex of cats (Lander *et al.* 1997; Kind *et al.* 2013).

Synaptic structure, which includes dendritic and axonal branching, as well as dendritic spine dynamics, plays crucial role in regulating plasticity. During early development, neurons undergo rapid changes in morphology to establish new synaptic connections (Lendvai *et al.* 2000; Holtmaat *et al.* 2005). During early development of mice before eye opening, plasticity of the visual cortex is driven by spontaneous activity (Toyoizumi *et al.* 2013; Chaudhury *et al.* 2016). In the subsequent development, visual inputs or sensory stimuli form the basis of activity-driven process crucial for the development of proper vision and may serve to fine-tune circuit connections by maturing inhibitory innervation (Hensch *et al.* 1998; Zheng *et al.* 1999; Fagiolini *et al.* 2004). Since PV+ neuron numbers were not affected by *Prmt8* knockout, increased complexity of pyramidal neurons in the visual cortex of *Prmt8*$^{-/-}$ mice could be a reflection of neuronal circuits locked in a juvenile state of reduced PV+ connectivity because of increased PNN formation. Consequently, visual acuity of *Prmt8*$^{-/-}$ mice are also poorer than the wild-type counterparts. It has been predicted that mice with decreased GABA-mediated synaptic inhibition will have lower visual acuity as they do not have the mechanisms necessary to depress poorly patterned visual input (Prusky and Douglas 2003). Despite a previous study reporting deficits in motor coordination and performance of *Prmt8*$^{-/-}$ mice (Kim *et al.* 2015), our data (Figure S2c and d) suggest that these mice do not perform significantly different in the water task as compared to wild-type mice.

Since fast-spiking basket cells that express PV provide the main source of perisomatic inhibition in the developing cortex (Klausberger *et al.* 2002), we looked at PV connections to see if we could explain the difference in dendritic morphology. Perisomatic inhibitory connections were reduced in *Prmt8*$^{-/-}$ mice as a result of increased PNNs. A previous report also found that TNR knockout mice displayed a reduction of perisomatic inhibition, and an increase in excitatory synaptic transmission in CA1 region of the hippocampus (Saghatelyan *et al.* 2001). Although perisomatic PV+ inhibitory synapses were reduced, it is still unclear if disinhibition occurred in visual circuits of *Prmt8*$^{-/-}$ mice. *In vivo* electrophysiological recordings may help to clarify if the excitatory-inhibitory balance of the visual circuits has been perturbed. In addition, maturation of intracortical inhibition is also closely associated with critical period progression (Fagiolini *et al.* 2004) and achieving sufficient inhibition is an important cue for the onset of critical period (Hensch *et al.* 1998; Fagiolini and Hensch 2000). Further work needs to be done to ascertain if this reduction of inhibitory synapses will affect ocular dominance plasticity in *Prmt8* null mice.

Acknowledgments and conflict of interest disclosure

We thank Dr. Newman Sze and his laboratory in National Technological University, Singapore for their assistance on the iTRAQ experiments and Dr. Joanna Holbrook for her advice on data analysis. This work was supported by the Agency for Science and Technology (A*STAR) intramural funding for the Integrative Neuroscience Programme, Singapore Institute for Clinical Sciences. The authors declared no competing interests.

All experiments were conducted in compliance with the ARRIVE guidelines.

Author contributions

P.K.M.L., W.W.B.G and J.C.G.S designed research; P.K.M.L. performed the experiments; P.K.M.L. and W.W.B.G. analyzed data; and P.K.M.L., W.W.B.G., J.C.G.S wrote the paper.

Supporting information

Additional Supporting Information may be found online in the supporting information tab for this article:

Figure S1. A wider and more relaxed search criteria on the raw MS spectra improved recovery of the 20 network-implicated proteins (c.f. Figure 2).

Figure S2. Training paradigm and performance of mice for the visual water task.

References

Alberini C. M. and Kandel E. R. (2015) The regulation of transcription in memory consolidation. *Cold Spring Harb. Perspect. Biol.* **7**, a021741.

Alpert A. J. (2007) Electrostatic repulsion hydrophilic interaction chromatography for isocratic separation of charged solutes and selective isolation of phosphopeptides. *Anal. Chem.* **80**, 62–76.

Altschul S. F., Gish W., Miller W., Myers E. W. and Lipman D. J. (1990) Basic local alignment search tool. *J. Mol. Biol.* **215**, 403–410.

Apweiler R., Bairoch A., Wu C. H. *et al.* (2004) UniProt: the universal protein knowledgebase. *Nucleic Acids Res.* **32**, D115–D119.

Bedford M. T. and Clarke S. G. (2009) Protein arginine methylation in mammals: who, what, and why. *Mol. Cell* **33**, 1–13.

Bjornson R. D., Carriero N. J., Colangelo C., Shifman M., Cheung K.-H., Miller P. L. and Williams K. (2008) X!!Tandem, an improved method for running X!tandem in parallel on collections of commodity computers. *J. Proteome Res.* **7**, 293–299.

Boyle E. I., Weng S., Gollub J., Jin H., Botstein D., Cherry J. M. and Sherlock G. (2004) GO:TermFinder–open source software for accessing Gene Ontology information and finding significantly enriched Gene Ontology terms associated with a list of genes. *Bioinformatics* **20**, 3710–3715.

Brakebusch C., Seidenbecher C. I., Asztely F., Rauch U., Matthies H., Meyer H., Krug M. *et al.* (2002) Brevican-deficient mice display impaired hippocampal CA1 long-term potentiation but show no obvious deficits in learning and memory. *Mol. Cell. Biol.* **22**, 7417–7427.

Brückner G., Grosche J., Schmidt S., Härtig W., Margolis R. U., Delpech B., Seidenbecher C. I., Czaniera R. and Schachner M. (2000) Postnatal development of perineuronal nets in wild-type mice and in a mutant deficient in tenascin-R. *J. Comp. Neurol.* **428**, 616–629.

Brunner A. M., Tweedie-Cullen R. Y. and Mansuy I. M. (2012) Epigenetic modifications of the neuroproteome. *Proteomics* **12**, 2404–2420.

Carulli D., Pizzorusso T., Kwok J. C. F., Putignano E., Poli A., Forostyak S., Andrews M. R., Deepa S. S., Glant T. T. and Fawcett J. W. (2010) Animals lacking link protein have attenuated perineuronal nets and persistent plasticity. *Brain* **133**, 2331–2347.

Chaudhury S., Sharma V., Kumar V., Nag T. C. and Wadhwa S. (2016) Activity-dependent synaptic plasticity modulates the critical phase of brain development. *Brain Dev.* **38**, 355–363.

Chittka A. (2010) Dynamic distribution of histone H4 arginine 3 methylation marks in the developing murine cortex. *PLoS ONE* **5**, e13807.

Dahlhaus M., Li K. W., van der Schors R. C., Saiepour M. H., van Nierop P., Heimel J. A., Hermans J. M., Loos M., Smit A. B. and Levelt C. N. (2011) The synaptic proteome during development and plasticity of the mouse visual cortex. *Mol. Cell Proteomics* **10**, M110.005413.

Dash P. K., Orsi S. A. and Moore A. N. (2009) Histone deactylase inhibition combined with behavioral therapy enhances learning and memory following traumatic brain injury. *Neuroscience* **163**, 1–8.

Engert F. and Bonhoeffer T. (1999) Dendritic spine changes associated with hippocampal long-term synaptic plasticity. *Nature* **399**, 66–70.

Fagiolini M. and Hensch T. K. (2000) Inhibitory threshold for critical-period activation in primary visual cortex. *Nature* **404**, 183–186.

Fagiolini M., Fritschy J. and Lo K. (2004) Specific GABA A circuits for visual cortical plasticity. *Science* **303**, 1681–1683.

Geer L. Y., Markey S. P., Kowalak J. A., Wagner L., Xu M., Maynard D. M., Yang X., Shi W. and Bryant S. H. (2004) Open mass spectrometry search algorithm. *J. Proteome Res.* **3**, 958–964.

Goh W. W. B. and Wong L. (2013) Networks in proteomics analysis of cancer. *Curr. Opin. Biotechnol.* **24**, 1122–1128.

Goh W. W. B. and Wong L. (2014) Computational proteomics: designing a comprehensive analytical strategy. *Drug Discov. Today* **19**, 266–274.

Goh W. W. B., Lee Y. H., Zubaidah R. M., Jin J., Dong D., Lin Q., Chung M. C. M. and Wong L. (2011) Network-based pipeline for analyzing MS data: an application toward liver cancer. *J. Proteome Res.* **10**, 2261–2272.

Goh W. W. B., Lee Y. H., Chung M. and Wong L. (2012) How advancement in biological network analysis methods empowers proteomics. *Proteomics* **12**, 550–563.

Goh W. W. B., Sergot M. J., Sng J. C. G. and Wong L. (2013a) Comparative network-based recovery analysis and proteomic profiling of neurological changes in valproic acid-treated mice. *J. Proteome Res.* **12**, 2116–2127.

Goh W. W. B., Wong L. and Sng J. C. G. (2013b) Contemporary network proteomics and its requirements. *Biology (Basel)* **3**, 22–38.

Goh W. W. B., Guo T., Aebersold R. and Wong L. (2015) Quantitative proteomics signature profiling based on network contextualization. *Biol. Direct* **10**, 71.

Grant S. G. N. (2012) Synaptopathies: diseases of the synaptome. *Curr. Opin. Neurobiol.* **22**, 522–529.

Guan J.-S., Haggarty S. J., Giacometti E., Dannenberg J.-H., Joseph N., Gao J., Nieland T. J. F. *et al.* (2009) HDAC2 negatively regulates memory formation and synaptic plasticity. *Nature* **459**, 55–60.

Gupta S., Kim S. Y., Artis S., Molfese D. L., Schumacher A., Sweatt J. D., Paylor R. E. and Lubin F. D. (2010) Histone methylation regulates memory formation. *J. Neurosci.* **30**, 3589–3599.

Hensch T. K. (2004) Critical period regulation. *Annu. Rev. Neurosci.* **27**, 549–579.

Hensch T. K., Fagiolini M., Mataga N., Stryker M. P., Baekkeskov S. and Kash S. F. (1998) Local GABA circuit control of experience-dependent plasticity in developing visual cortex. *Science* **282**, 1504–1508.

Holtmaat A. J. G. D., Trachtenberg J. T., Wilbrecht L., Shepherd G. M., Zhang X., Knott G. W. and Svoboda K. (2005) Transient and persistent dendritic spines in the neocortex in vivo. *Neuron* **45**, 279–291.

Ippolito D. M. and Eroglu C. (2010) Quantifying synapses: an immunocytochemistry-based assay to quantify synapse number. *J. Vis. Exp.* **45**, e2270.

Jahan S. and Davie J. R. (2015) Protein arginine methyltransferases (PRMTs): role in chromatin organization. *Adv. Biol. Regul.* **57**, 173–184.

Ju W., Morishita W., Tsui J., Gaietta G., Deerinck T. J., Adams S. R., Garner C. C., Tsien R. Y., Ellisman M. H. and Malenka R. C. (2004) Activity-dependent regulation of dendritic synthesis and trafficking of AMPA receptors. *Nat. Neurosci.* **7**, 244–253.

Karp N. A., Huber W., Sadowski P. G., Charles P. D., Hester S. V. and Lilley K. S. (2010) Addressing accuracy and precision issues in iTRAQ quantitation. *Mol. Cell Proteomics* **9**, 1885–1897.

Kim J.-D., Park K.-E., Ishida J. *et al.* (2015) PRMT8 as a phospholipase regulates Purkinje cell dendritic arborization and motor coordination. *Sci. Adv.* **1**, e1500615.

Kind P. C., Sengpiel F., Beaver C. J., Crocker-Buque A., Kelly G. M., Matthews R. T. and Mitchell D. E. (2013) The development and activity-dependent expression of aggrecan in the cat visual cortex. *Cereb. Cortex* **23**, 349–360.

Klausberger T., Roberts J. D. B. and Somogyi P. (2002) Cell type- and input-specific differences in the number and subtypes of synaptic GABA(A) receptors in the hippocampus. *J. Neurosci.* **22**, 2513–2521.

Korzus E., Rosenfeld M. G. and Mayford M. (2004) CBP histone acetyltransferase activity is a critical component of memory consolidation. *Neuron* **42**, 961–972.

Kousaka A., Mori Y., Koyama Y., Taneda T., Miyata S. and Tohyama M. (2009) The distribution and characterization of endogenous protein arginine N-methyltransferase 8 in mouse CNS. *Neuroscience* **163**, 1146–1157.

Lander C., Kind P., Maleski M. and Hockfield S. (1997) A family of activity-dependent neuronal cell-surface chondroitin sulfate proteoglycans in cat visual cortex. *J. Neurosci.* **17**, 1928–1939.

Lau L. W., Cua R., Keough M. B., Haylock-Jacobs S. and Yong V. W. (2013) Pathophysiology of the brain extracellular matrix: a new target for remyelination. *Nat. Rev. Neurosci.* **14**, 722–729.

Lendvai B., Stern E. A., Chen B. and Svoboda K. (2000) Experience-dependent plasticity of dendritic spines in the developing rat barrel cortex in vivo. *Nature* **404**, 876–881.

Levenson J. M., O'Riordan K. J., Brown K. D., Trinh M. A., Molfese D. L. and Sweatt J. D. (2004) Regulation of histone acetylation during memory formation in the hippocampus. *J. Biol. Chem.* **279**, 40545–40559.

Lin Y., Tsai Y.-J., Liu Y.-F., Cheng Y.-C., Hung C.-M., Lee Y.-J., Pan H. and Li C. (2013) The critical role of protein arginine methyltransferase prmt8 in zebrafish embryonic and neural development is non-redundant with its paralogue prmt1. *PLoS ONE* **8**, e55221.

Liu X.-A., Kadakkuzha B., Pascal B., Steckler C., Akhmedov K., Yan L., Chalmers M. and Puthanveettil S. V. (2014) New approach to capture and characterize synaptic proteome. *Proc. Natl Acad. Sci. USA* **111**, 16154–16159.

Lluch-Senar M., Mancuso F. M., Climente-González H., Peña-Paz M. I., Sabido E. and Serrano L. (2016) Rescuing discarded spectra: full comprehensive analysis of a minimal proteome. *Proteomics* **16**, 554–563.

Lundell A., Olin A. I., Mörgelin M., al-Karadaghi S., Aspberg A. and Logan D. T. (2004) Structural basis for interactions between tenascins and lectican C-type lectin domains: evidence for a crosslinking role for tenascins. *Structure* **12**, 1495–1506.

Ma D. K., Jang M.-H., Guo J. U., Kitabatake Y., Chang M.-L., Pow-Anpongkul N., Flavell R. A., Lu B., Ming G.-L. and Song H. (2009) Neuronal activity-induced Gadd45b promotes epigenetic DNA demethylation and adult neurogenesis. *Science* **323**, 1074–1077.

McCloy R. A., Rogers S., Caldon C. E., Lorca T., Castro A. and Burgess A. (2014) Partial inhibition of Cdk1 in G 2 phase overrides the SAC and decouples mitotic events. *Cell Cycle* **13**, 1400–1412.

Miller C. A. and Sweatt J. D. (2007) Covalent modification of DNA regulates memory formation. *Neuron* **53**, 857–869.

Montojo J., Zuberi K., Rodriguez H., Bader G. D. and Morris Q. (2014) GeneMANIA: Fast gene network construction and function prediction for Cytoscape.. *F1000Res.* **3**, 153.

Morawski M., Dityatev A., Hartlage-Rübsamen M., Blosa M., Holzer M., Flach K., Pavlica S. *et al.* (2014) Tenascin-R promotes assembly of the extracellular matrix of perineuronal nets via clustering of aggrecan. *Philos. Trans. R. Soc. Lond. B Biol. Sci.* **369**, 20140046.

Morris N. P. and Henderson Z. (2000) Perineuronal nets ensheath fast spiking, parvalbumin-immunoreactive neurons in the medial septum/diagonal band complex. *Eur. J. Neurosci.* **12**, 828–838.

Mostafavi S., Ray D., Warde-Farley D., Grouios C. and Morris Q. (2008) GeneMANIA: a real-time multiple association network integration algorithm for predicting gene function. *Genome Biol.* **9** (Suppl 1), S4.

Mouw J. K., Ou G. and Weaver V. M. (2014) Extracellular matrix assembly: a multiscale deconstruction. *Nat. Rev. Mol. Cell Biol.* **15**, 771–785.

Nesvizhskii A. I. (2007) Protein identification by tandem mass spectrometry and sequence database searching. *Methods Mol. Biol.* **367**, 87–119.

Oliveros J. C. (2015) Venny. An interactive tool for comparing lists with Venn's diagrams.

Pesheva P. and Probstmeier R. (2000) The yin and yang of tenascin-R in CNS development and pathology. *Prog. Neurobiol.* **61**, 465–493.

Pizzorusso T., Medini P., Berardi N., Chierzi S., Fawcett J. W. and Maffei L. (2002) Reactivation of ocular dominance plasticity in the adult visual cortex. *Science* **298**, 1248–1251.

Prusky G. T. and Douglas R. M. (2003) Developmental plasticity of mouse visual acuity. *Eur. J. Neurosci.* **17**, 167–173.

Prusky G. T. and Douglas R. M. (2004) Characterization of mouse cortical spatial vision. *Vision. Res.* **44**, 3411–3418.

Prusky G. T., West P. W. and Douglas R. M. (2000) Behavioral assessment of visual acuity in mice and rats. *Vision. Res.* **40**, 2201–2209.

Prusky G. T., Silver B. D., Tschetter W. W., Alam N. M. and Douglas R. M. (2008) Experience-dependent plasticity from eye opening enables lasting, visual cortex-dependent enhancement of motion vision. *J. Neurosci.* **28**, 9817–9827.

Putignano E., Lonetti G., Cancedda L., Ratto G., Costa M., Maffei L. and Pizzorusso T. (2007) Developmental downregulation of histone posttranslational modifications regulates visual cortical plasticity. *Neuron* **53**, 747–759.

Putthoff P., Akyüz N., Kutsche M., Zardi L., Borgmeyer U. and Schachner M. (2003) Structure of the murine tenascin-R gene and functional characterisation of the promoter. *Biochem. Biophys. Res. Commun.* **308**, 940–949.

Raab-Graham K. F., Haddick P. C. G., Jan Y. N. and Jan L. Y. (2006) Activity- and mTOR-dependent suppression of Kv1.1 channel mRNA translation in dendrites. *Science* **314**, 144–148.

Rosenberg T., Gal-Ben-Ari S., Dieterich D. C., Kreutz M. R., Ziv N. E., Gundelfinger E. D. and Rosenblum K. (2014) The roles of protein expression in synaptic plasticity and memory consolidation. *Front. Mol. Neurosci.* **7**, 86.

Ross P. L., Huang Y. N., Marchese J. N. *et al.* (2004) Multiplexed protein quantitation in *Saccharomyces cerevisiae* using amine-reactive isobaric tagging reagents. *Mol. Cell Proteomics* **3**, 1154–1169.

Saghatelyan A. K., Dityatev A., Schmidt S., Schuster T., Bartsch U. and Schachner M. (2001) Reduced perisomatic inhibition, increased excitatory transmission, and impaired long-term potentiation in mice deficient for the extracellular matrix glycoprotein tenascin-R. *Mol. Cell Neurosci.* **17**, 226–240.

Satterlee J. S., Beckel-Mitchener A., Little R., Procaccini D., Rutter J. L. and Lossie A. C. (2015) Neuroepigenomics: resources, obstacles, and opportunities. *Neuroepigenetics* **1**, 2–13.

Schneider C. A., Rasband W. S. and Eliceiri K. W. (2012) NIH Image to ImageJ: 25 years of image analysis. *Nat. Methods* **9**, 671–675.

Specht M., Kuhlgert S., Fufezan C. and Hippler M. (2011) Proteomics to go: proteomatic enables the user-friendly creation of versatile MS/MS data evaluation workflows. *Bioinformatics* **27**, 1183–1184.

Sutton M. A., Wall N. R., Aakalu G. N. and Schuman E. M. (2004) Regulation of dendritic protein synthesis by miniature synaptic events. *Science* **304**, 1979–1983.

Sutton M. A., Ito H. T., Cressy P., Kempf C., Woo J. C. and Schuman E. M. (2006) Miniature neurotransmission stabilizes synaptic function via tonic suppression of local dendritic protein synthesis. *Cell* **125**, 785–799.

Taneda T., Miyata S., Kousaka A., Inoue K., Koyama Y., Mori Y. and Tohyama M. (2007) Specific regional distribution of protein arginine methyltransferase 8 (PRMT8) in the mouse brain. *Brain Res.* **1155**, 1–9.

Toyoizumi T., Miyamoto H., Yazaki-Sugiyama Y., Atapour N., Hensch T. K. and Miller K. D. (2013) A theory of the transition to critical period plasticity: inhibition selectively suppresses spontaneous activity. *Neuron* **80**, 51–63.

Wang D. and Fawcett J. (2012) The perineuronal net and the control of CNS plasticity. *Cell Tissue Res.* **349**, 147–160.

Weber P., Bartsch U., Rasband M. N. *et al.* (1999) Mice deficient for tenascin-R display alterations of the extracellular matrix and

decreased axonal conduction velocities in the CNS. *J. Neurosci.* **19**, 4245–4262.

Wolf S. S. (2009) The protein arginine methyltransferase family: an update about function, new perspectives and the physiological role in humans. *Cell. Mol. Life Sci.* **66**, 2109–2121.

Yang Y. and Bedford M. T. (2013) Protein arginine methyltransferases and cancer. *Nat. Rev. Cancer* **13**, 37–50.

Zheng W. and Knudsen E. I. (1999) Functional selection of adaptive auditory space map by GABAA-mediated inhibition. *Science* **284**, 962–965.

Zhou X. H., Brakebusch C., Matthies H. *et al.* (2001) Neurocan is dispensable for brain development. *Mol. Cell. Biol.* **21**, 5970–5978.